Corrosion behaviour of Mg–Al alloys with Al thermal spray coatings in humid and saline environments

R. Arrabal[a,*], A. Pardo[a], M.C. Merino[a], S. Merino[b], P. Casajús[a], M. Mohedano[a], P. Rodrigo[c]

[a]*Departamento de Ciencia de Materiales, Facultad de Químicas, Universidad Complutense, 28040, Madrid, Spain*

[b]*Departamento de Tecnología Industrial, Universidad Alfonso X El Sabio, 28691, Villanueva de la Cañada, Madrid, Spain*

[c]*Departamento de Ciencia e Ingeniería de Materiales, ESCET, Universidad Rey Juan Carlos, 28933, Móstoles, Madrid, Spain*

[*]Corresponding author. Tel: 34 1 3945227; Fax: 34 1 3944357

E–mail: raularrabal@quim.ucm.es

ABSTRACT

The corrosion behaviour of thermal spray Al coatings deposited on AZ31, AZ80 and AZ91D Mg–Al alloys was evaluated in salt water (3.5 wt.% NaCl), neutral salt fog (ASTM B 117) and high relative humidity (98% RH, 50 ºC) environments. The changes in the morphology and corrosion behaviour of the Al coatings induced by cold–pressing post–treatment were also examined. In chloride–containing environments, the presence of interconnected pores in the as–sprayed Al coatings facilitated the galvanic acceleration of the corrosion of the magnesium substrates. The cold–pressed Al coatings revealed improved corrosion behaviour associated with a lower level of porosity. In high humidity environment, even though the corrosion rates for all the examined materials were lower than in the case of salt fog, similar corrosion features were observed; formation of hydromagnesite on the surface of untreated materials, galvanic corrosion in the Al–TS specimens and almost negligible corrosion attack of the Al coating with formation of bayerite (β–$Al_2O_3 \cdot 3H_2O$) in the case of the cold–pressed specimens.

Keywords: aluminium coatings; aqueous environments; atmospheric causes; chloride; corrosion resistance; thermal spraying.

1. Introduction

Aluminium is the most important alloying element for magnesium, with commercial Mg–Al alloys usually containing less than 10 wt.% Al. The addition of this alloying element results in better castability and an increase of ambient tensile, compressive, and fatigue strength. In general, corrosion resistance of Mg–Al alloys increases with the addition of aluminium.[1–5] However, for the same alloy composition, significant variations in the corrosion mechanism and corrosion rate values may be observed due to different impurity levels, manufacturing processes and/or alloy microstructure.[6]

In humid and aqueous environments, the corrosion behaviour of Mg–Al alloys greatly depends on the presence or not of Cl^- ions and the morphology and distribution of the β–$Mg_{17}Al_{12}$ phase.[7–10] In chloride–containing or saline environments, especially in aqueous solutions, magnesium is highly susceptible to corrosion attack due to the breakdown of the partially protective film on the magnesium surface,[11] whereas in humid environments, under thin electrolyte layers, the anodic process is generally diminished compared to a bulk electrolyte in aqueous solutions.[12] The corrosion resistance of magnesium alloys is comparable to that of mild steel in rural and industrial environments.[13]

Some of the current applications of magnesium alloys in the transport sector, where their high specific strength and low density can be used to great advantage, include gearboxes, engine blocks, crankcases, instrument panels, seat frames…[14] These are mainly indoor structures and the corrosion resistance is often not critical. However, in order to broaden the structural applications of magnesium alloys under more aggressive environments, surface treatments are needed.

Conversion coatings and anodizing treatments are commonly used for magnesium alloys.[15] Conversion coatings enclose some limitations which include different treatments needed depending on the alloy composition and the frequent use of chromates that are now being restricted due to high environmental risk of Cr(VI).[16, 17] Anodizing treatments are often inadequate due to the large size of the specimens and/or by the non–environmental friendliness of the composition of the electrolyte, which often contains fluorides or chromates.[18]

Thermal spray coatings offer an alternative to the above methods. The main advantage of this technique is the ability to apply a wide range of functional coatings on many different substrates without significantly heating them.[19] Previous studies on the fabrication of Al coatings on magnesium substrates have shown that thermal spray is a simple method, economical and pollution free that favours recycling of magnesium, and could improve the corrosion resistance of magnesium alloy substrates if appropriate post–treatments are applied.[20–27]

In the present study, the corrosion behaviour of thermal spray Al coatings deposited on Mg–Al alloys was evaluated in humid and saline environments. The findings revealed considerable corrosion protection for all the examined magnesium alloys after application of a cold–pressing post–treatment.

2. Experimental

2.1. Test Materials

The chemical compositions of the tested magnesium alloys are given in Table 1. Unalloyed Mg was used as the reference material. Pure Mg and AZ31 alloy were fabricated in wrought condition and supplied in plates of 3 mm thickness, whereas the AZ80 and AZ91D alloys were manufactured by a casting process, and used in the form of billets of 10 mm thickness and 300 and 250 mm in diameter respectively. All the materials were supplied by Magnesium Elektron Ltd.

2.2. Al coatings

Prior to the thermal spray process, the surfaces of the magnesium materials were sand–blasted with corundum of 1 mm mean diameter. Aluminium spray coatings were then applied on the magnesium substrates using Al powder with a particle average size of 125 μm (Castolin: 99.5% Al rich) and a flame spray gun (Castolin DS8000 system with a SSM40 modulus) that provided a thermal power of 28 kW by mixing oxygen at 4 bar and 2000 L h^{-1} with acetylene at 0.7 bar and 1800 L h^{-1}. The processing parameters were: spray distance of 20 cm; neutral flame (*i.e.* balanced amounts of oxygen and acetylene to get full combustion); transversal gun displacement over the sample surface of 150 cm min^{-1}; material feeding rate of ~ 1.0 g s^{-1} and average particle speed of 300 m s^{-1}. These parameters corresponded to a low velocity oxy–fuel (LVOF) process that is known to be a cheaper alternative than other thermal spray processes. However, as a consequence of the lower particle velocities obtained, the coatings generally reveal lower bond strength, higher porosity and a lower overall cohesive (interparticle) strength. In order to reduce the level of porosity of these coatings, a cold–pressing post–treatment was carried out at a pressure of 32 MPa for 3 min at room temperature. For all the experiments, duplicate specimens were prepared to guarantee the reliability of the results.

2.3. Specimen examination

For metallographic characterization of coated specimens, cross–sections were wet ground through successive grades of silicon carbide abrasive paper, from P120 to P2000, followed by diamond finishing to 0.1 μm. Two etching reagents were used: a) Nital, 5 mL HNO_3 + 95 mL ethanol, to reveal the constituents and general microstructure of Mg, AZ80 and AZ91D materials and b) Vilella reagent, 0.6 g picric acid + 10 mL ethanol + 90 mL H_2O, to reveal grain boundaries of AZ31 alloy. The constituents were examined by SEM using a JEOL JSM–6400 microscope equipped with Oxford Link EDX microanalysis hardware. Phase composition was investigated by low–angle XRD using a Philips X´Pert diffractometer ($K_\alpha Cu$ = 1.54056 Å).

2.4. Electrochemical measurements in 3.5 wt.% NaCl

The electrochemical behaviour of investigated materials was examined using an AUTOLAB model PGSTAT 30 computer–controlled potentiostat and a conventional three–electrode cell, employing a graphite counter electrode and a silver–silver chloride reference electrode (SSE). Solution concentration inside the reference electrode compartment was KCl 3M, with a potential of 0.197 V with respect to standard hydrogen electrode. The working electrode with 0.28 cm^2 of immersed area was the test material and the test solution was naturally aerated 3.5 wt.% NaCl solution at room temperature (22 ºC).

Anodic polarization measurements were carried out at a scan rate of 0.3 mV s^{-1}, from –100 mV with respect to the corrosion potential (E_{corr}) up to a maximum anodic corrosion current of 5 mA cm^{-2}. For cyclic polarization, the scan direction was reversed when the samples reached the anodic corrosion current of 5 mA cm^{-2} and the potential was scanned back to the starting potential.

2.5. Gravimetric measurements

Gravimetric measurements were performed using specimens of working area of ~ 15 cm^2 that were weighed before and after the tests using a Sartorius BP 211D scale with an accuracy of 0.00001 g. Mass changes were calculated according to the expression $(M_f - M_i)/A$, where M_f is the final mass, M_i the initial mass and A the exposed surface area.

– *Salt fog environment*

The specimens were hung in a CCl cabinet with a nylon thread and exposed to a 5 wt.% NaCl spray (pH 6.5–7.2) during 21 days. As recommended by ASTM B 117 standard, atomized air pressure of the saline solution was maintained in the range of 69 to 172 kN m^{-2} and the temperature inside the cabinet at 35 ± 1 ºC. At the end of the tests, the specimens were washed with water below 38 ºC to remove the saline deposits, dried in hot air and weighed.

– *High humidity environment*

The high relative humidity tests consisted of 24 h cycles performed in a saturated water vapour at 98% RH and 50 ± 1 ºC during 28 days simulated by a humidity condensation cabinet CCK 300 (Dycometal). The temperature and the humidity were verified using a digital thermometer and hygrometer. At the end of the tests, the specimens were rinsed with deionized water, dried in warm air and weighed.

2.6. Characterization of corrosion products

The tested specimens were examined by SEM in order to study the morphology and evolution of corrosion products formed on the material surface. Composition of the corrosion layer was examined by low–angle XRD.

3. Results

3.1. Microstructural characterization of the coatings

Microstructural characterization of the as–received materials can be found elsewhere.[28] Figures 1a–f show the backscattered scanning electron (BSE) micrographs of the cross–sections of as–sprayed (Al–TS) and cold–pressed Al coatings (Al–TS+CP). The Al–TS coatings revealed an average thickness of 600 ± 100 µm with a very rough surface, which is characteristic of LVOF coatings. Interconnected pores were randomly distributed within the as–sprayed coatings and the substrate/coating interface revealed poor bonding and some roughness due to the sand blasting pre–treatment (Fig. 1a–c, Fig. 2a, Fig. 2c).

The cold–pressing post–treatment under 32 MPa at room temperature produced more compact Al coatings with a thickness of 500 ± 25 µm (Fig. 1d–f). The Al–TS+CP coatings revealed smoother surfaces and were more homogeneous with improved bonding at the coating/substrate interface and reduced level of porosity (Fig. 1d–f, Fig. 2b, Fig. 2d). However, the presence of interconnected micro–pores between the deposited splats cannot be completely excluded.

The presence of deformed microstructures or inter–diffusion or compound layers was not observed between the Al coatings and the magnesium substrates (Fig. 2c, Fig. 2d). These features differed

from other thermal spray Al coatings on magnesium alloys with heat post–treatments, where secondary microstructures are commonly observed.[27]

3.2. Electrochemical results

Figure 3 and Tables 2 and 3 disclose the polarization curves and electrochemical data of studied materials after immersion in 3.5 wt.% NaCl solution at room temperature for 1 h. The deposition of Al on the magnesium substrates shifted the corrosion potential (E_{corr}) from ~ – 1.5 V_{SSE} to – 1.1 V_{SSE}. Therefore, the coated specimens may reveal galvanic corrosion if the Al coatings are permeable to the aggressive solution. The corrosion current density, i_{corr}, of untreated alloys decreased with higher aluminium content in the composition of the alloys, from ~ 4.3×10^{-3} A cm^{-2} for pure Mg, to 1.5–2.5×10^{-5} A cm^{-2} for magnesium alloys containing 8–9 wt.% aluminium.[5] The i_{corr} values of the Al–TS specimens were in the range of 1.0×10^{-5} A cm^{-2} to 1.7×10^{-4} A cm^{-2}, suggesting low corrosion protection of the Al–TS coatings and possible galvanic corrosion of the substrates as the corrosion rate of these specimens was similar and, in some cases, higher than that of untreated ones. The cold–pressed specimens revealed higher E_{corr} values (~ – 1.1 V_{SSE}) and lower corrosion rates than those of untreated specimens by 1 to 3 orders of magnitude (~ 10^{-6} A cm^{-2}), which were similar to those reported for other Al coatings deposited on magnesium alloys.[29, 30] The Al–TS+CP specimens also revealed a passive range of 0.5 V_{SSE} between the E_{corr} and the pitting potential (E_{pit}) at ~ – 0.6 V_{SSE} and a repassivation potential (E_{rep}) around – 0.75 V_{SSE}. These electrochemical data were similar for all the Al–TS+CP specimens, indicating that the corrosion behaviour in 3.5 wt.% NaCl was irrespective of the composition or microstructure of the magnesium substrate after the application of the cold–pressing post–treatment (Tables 2 and 3).

Similar conclusions were obtained from the comparison of the polarization resistance (R_p) values (Table 2). The Al–TS+CP specimens revealed higher R_p values (~ 16000 Ω cm^2) than the Al–TS (~ 150 Ω cm^2) and untreated specimens (~ 20–5300 Ω cm^2).

3.3. Gravimetric results

– *Salt fog environment*

Figure 4 shows the gravimetric results of studied materials exposed to salt fog environment for 21 days. The untreated pure Mg and AZ31 materials exhibited significant mass loss, indicative of their low corrosion resistance in this environment. The AZ80 and AZ91D magnesium alloys, with higher Al content (8–9 wt.%), revealed relatively minor mass gain values (21 days, 16 mg cm^{-2}) accompanied by formation of corrosion products of white colour, which possibly were magnesium oxides and/or hydroxides due to the high reactivity of magnesium materials in chloride–containing environments. The Al–TS specimens revealed poor corrosion performance in salt fog environment and the mass gain values were in the interval between 35 mg cm^{-2} and 70 mg cm^{-2} after 21 days. On the other hand, the Al–TS+CP specimens revealed the best corrosion performance with relatively low mass gain values (~ 7 mg cm^{-2}) at the end of the test.

– *High humidity environment*

Figure 5 discloses the gravimetric results of tested materials exposed to 98% RH at 50 ºC for 28 days. The untreated materials revealed minor corrosion with mass gain values up to 0.5 mg cm^{-2} for pure Mg and the AZ31 alloy and up to 0.2 mg cm^{-2} for the AZ80 and AZ91D alloys after 28 days. This mass gain is normally associated with the absorption of H_2O and CO_2 and formation of a corrosion layer on the surface.[28] In consistency with the electrochemical tests in 3.5 wt.% NaCl and the gravimetric measurements in salt fog, increasing amounts of aluminium in the composition of the magnesium substrate reduced the magnitude of the corrosion attack.

The as–sprayed Al coatings were not protective and high mass gain values were observed for all the Al–TS specimens after 28 days (1.24 mg cm^{-2}), whereas the Al–TS+CP specimens, similarly to the untreated materials, revealed negligible mass gain after exposure to 98% RH–50 ºC for 28 days (0.3 mg cm^{-2}).

Table 4 and 5 show the kinetic laws calculated from the gravimetric measurements using a linear ($y = b \cdot t$; y: mass gain; t: time) or parabolic expression ($y^2 = b \cdot t$). In salt fog environment, the increase in aluminium content in the bulk composition of the magnesium alloy caused a decrease in the corrosion rate by up to 275 times. The Mg and AZ31 materials with the as–sprayed Al coatings followed a linear trend, whereas with the AZ80 and AZ91D substrates a parabolic trend was observed. This was possibly related to limited diffusion of the aggressive species through the corrosion products layer. For the Al–TS+CP specimens, the corrosion rate was identical for all the substrates, indicating that the cold–pressing post–treatment produced a more effective barrier between the magnesium substrate and the environment. In high humidity environment, all the specimens followed linear kinetics. The Al–TS specimens revealed higher corrosion rates (~ 4 ×

10^{-2} mg cm^2 d^{-1}) than the untreated and Al–TS+CP specimens, which exhibited very similar values (~ 1–2 × 10^{-2} mg cm^2 d^{-1}).

3.4. Characterization of corrosion products

– Salt fog environment

The scanning electron micrographs of the plan views of the untreated magnesium alloys after exposure in salt fog for 21 days revealed considerable corrosion attack with formation of an uneven corrosion layer that was less evident in the case of the materials with high aluminium content (AZ80 and AZ91D) (Fig. 6a, Fig. 6b). (The pure Mg specimen was dissolved after 7 days in salt fog). The examination of the cross–sections of the untreated materials after 21 days in salt fog revealed the heterogeneity of the corrosion attack with deep pits in some areas of the surface (Fig. 7). In unpublished work of the authors, the initiation sites of corrosion were found to depend on the aluminium content and alloy microstructure.

The outer surface of the Al–TS and Al–TS+CP specimens exhibited slight corrosion attack and suggested better corrosion performance compared with the untreated specimens. Most likely, the corrosion products were rich in aluminium due to the corrosion susceptibility of this metal when it is exposed to chloride–containing environments (Figs. 6c–f).[31, 32] SEM characterization of the cross–section of the Al–TS specimens after 21 days in salt fog indicated that the above plan views were ambiguous and significant corrosion of the magnesium substrates occurred (Fig. 8). X-ray elemental maps of Mg, Al and O suggested that the corrosion products at the interface mainly consisted of magnesium oxides/hydroxides. In the case of the Al–TS+CP specimens a 10 μm aluminium–rich corrosion layer was formed on the outermost surface of the Al coating (Fig. 9).

Thus, the effectiveness of the Al coatings was greatly enhanced after the cold–pressing post–treatment due to the elimination of the interconnected pores, which in the case of the Al–TS specimens facilitated the penetration of the corrosive medium and the galvanic acceleration of the corrosion of the magnesium substrates.

Figure 10 discloses the low angle XRD study (incident angle 1°) of the investigated materials after exposure to salt fog environment for 21 days. For the untreated materials, the main corrosion products were magnesium hydroxide (brucite ($Mg(OH)_2$) and hydrated magnesium carbonate hydroxide (hydromagnesite $Mg_5(CO_3)_4(OH)_2 \cdot 4H_2O$). The latter showed higher intensity peaks for the AZ80 and AZ91D alloys. On the other hand, the majority of Al coated specimens revealed bayerite (β–$Al_2O_3 \cdot 3H_2O$) on the outermost surface of the coating. In the case of the Al–TS specimens, magnesium corrosion products, most likely $Mg(OH)_2$, were also found at the coating/substrate interface (Fig. 8), though they were not observed by the low–angle XRD study since it only detects phases on the surface. XRD is limited to crystalline phases and by the minimal thickness of the examined layer, thus, other corrosion products such as nesquehonite ($MgCO_3.3H_2O$), magnesium carbonate chloride hydroxide hydrate ($MgCl_2 2MgCO_3(OH)_2.6H_2O$, $Mg(OH)_2$, hydrotalcite ($Mg_6Al_2(OH)_{16}CO_3.4H_2O$) and $Al(OH)_3$ may also be present as amorphous material[19].

– *High humidity environment*

Examination of the surface of the untreated magnesium alloys after exposure to high humidity environment for 28 days revealed slight degree of corrosion with only a small amount of corrosion products (Fig. 11a, Fig. 11b). In unpublished work of the authors, the initiation sites of corrosion

were found to be related to the alloy microstructure and aluminium content. According to the SEM images (Fig. 11c–f), the surface of Al–coated specimens remained almost unchanged after exposure to the high humidity environment for 28 days.

For the untreated materials, XRD measurements following exposure to 98% RH and 50 ºC (Fig. 12) also revealed hydromagnesite and brucite as the main corrosion products, but in this case the $Mg(OH)_2$ peaks revealed lower intensity. The XRD patterns of the Al–TS specimens only showed Al peaks with no signs of corrosion products, whereas the Al–TS+CP specimens revealed small intensity peaks of bayerite (Fig. 12). These results suggested that, for the Al–TS specimens, which revealed relatively high mass gain values, the corrosion attack occurred preferentially in the inner regions of the coating and/or at the coating/substrate interface, although this could not be confirmed by SEM examination.

4. Discussion

In the present study, accelerated corrosion tests were used for evaluation of the corrosion behaviour of Mg–Al alloys with thermal spray Al coatings. According to the electrochemical and gravimetric measurements, the untreated AZ31, AZ80 and AZ91D magnesium alloys revealed severe corrosion attack in chloride–containing environments. This was also confirmed from the high pH level (pH 10.8) of the 3.5 wt.% NaCl solution after immersion for 1 h (Fig. 13). It is well-known that pH increases along with magnesium corrosion due to the generation of OH^- ions.[33]

After protracted times in saline environments, the morphology of the corrosion attack in the untreated materials was found to be heterogeneous, with formation of uneven corrosion layers and relatively deep pits (Fig. 6, Fig. 7). XRD peaks of the corrosion products, formed after 21 days in

salt fog, were assigned to brucite and hydromagnesite (Fig. 10). Brucite ($Mg(OH)_2$) is the most common corrosion product in magnesium alloys.[6] However, in the presence of atmospheric CO_2, brucite can react with $Mg(OH)_2$ to form magnesite ($MgCO_3$), which together with water will form hydromagnesite.[34]

In high humidity environment, all the untreated alloys showed minor corrosion attack. Similarly to the results in saline environments, for the untreated materials, the AZ80 and AZ91D magnesium alloys, with 8–9 wt.% Al, revealed the lowest corrosion rates (~ 26 μm/year). These values were somewhat higher than those obtained by Godard[13] and Southwell[35] for the AZ91D alloy exposed to rural (4–12 μm/year) and marine (22–19 μm/year) atmospheres. This was likely due to the higher humidity (98% RH) and temperature (50 ºC) used in this study. The XRD patterns also pointed out hydromagnesite as the main corrosion product for the untreated materials after exposure to 98% RH–50 ºC for 28 days, whereas $Mg(OH)_2$ peaks revealed lower intensity compared with the specimens exposed to salt fog.

Previous results by Jönsson[34, 36] also revealed hydromagnesite as the main corrosion product on the surface of Mg–Al alloys exposed to field and laboratory conditions, whereas brucite ($Mg(OH)_2$) was only detected for the latter conditions.[36] This was explained by the difference in the facility of transport of CO_2 through the corrosion products. Therefore, according to the XRD results, it is considered here that CO_2 penetrated more easily through the whole layer of corrosion products formed in high humidity environment compared with the corrosion products formed in salt fog. The formation of magnesium carbonates has been reported to reduce the susceptibility to localized

corrosion of magnesium exposed to humid air.[37] Thus, the improved corrosion performance of the AZ80 and AZ91D alloys compared with the AZ31 and pure Mg materials in high humidity environment may be associated with the different proportion of hydromagnesite on the surface. In line with this hypothesis, XPS analysis of the air formed film on these alloys revealed that the higher the amount of aluminium in solid solution the higher is the amount of magnesium carbonate species formed on the surface.[28] Other possible explanations include the formation of an aluminium rich layer[38] or the β–phase acting as a barrier against corrosion in two–phase Mg–Al alloys.[4]

Possibly, the observed corrosion behaviour of the examined magnesium alloys was a combination of all these factors.

The Al coatings deposited by a LVOF process followed by a cold–pressing post–treatment reduced the corrosion rate of the Mg–Al alloys exposed to salt fog and high humidity environments to ~ 630 μm/year and ~ 30 μm/year respectively. These values were of the same order as those observed for aluminium alloys under the same conditions.[39] Likewise, electrochemical results in 3.5 wt.% NaCl revealed lower corrosion rates than those of untreated specimens by 1 to 3 orders of magnitude (~ 10^{-6} A cm^{-2}) and a passive region in the anodic branch. These results suggested minor corrosion of the Al–TS+CP coatings with negligible participation of the magnesium substrates in the corrosion process. This was confirmed by SEM and XRD results, which revealed aluminium corrosion products (bayerite), characteristic of aluminium alloys[40], in the outermost surface of the coatings. On the other hand, the as–sprayed Al coatings did not provide effective protection and revealed much higher corrosion rates in the electrochemical and gravimetric measurements. This was also observed from the pH values after immersion in 3.5 wt.% NaCl for 1h (Fig. 13). SEM images and

X–ray elemental maps of Mg, O and Al indicated that the as–sprayed Al coatings were permeable to the aggressive solution, due to the presence of interconnected pores, and facilitated the galvanic corrosion of the substrates as predicted by the different corrosion potential values between the Al coating and the magnesium substrates (Fig. 8). Similar features were observed by Lugscheider[41] for thermal spray Al coatings deposited on the AZ91D alloy and immersed in 3% NaCl solution for 19 h. It should also be noted that the corrosion rate values of the Al–TS specimens estimated by electrochemical measurements are likely to be inexact due to galvanic coupling between substrate and coating.

5. Conclusions

1. The AZ31, AZ80 and AZ91D magnesium alloys revealed severe and minor corrosion in saline and high humidity environments respectively. The corrosion products mainly consisted of $Mg(OH)_2$ and $Mg_5(CO_3)_4(OH)_2 \cdot 4H_2O$ after exposure for protracted times. The lowest corrosion rates were observed for the alloys with higher aluminium content (Salt fog – AZ80: 0.2 mg cm^{-2} d^{-1} and AZ91D 1.6 mg cm^{-2} d^{-1}; humid air – AZ80: 1.2×10^{-2} mg cm^{-2} d^{-1} and AZ91D: 1.3×10^{-2} mg cm^{-2} d^{-1}).

2. The as–sprayed aluminium coatings revealed high number of interconnected pores between the deposited splats of aluminium. Ready penetration of the aggressive species towards the magnesium substrate occurred, followed by galvanic corrosion attack at the substrate/coating interface motivated by the different nobility of aluminium and magnesium. This was more evident in chloride–containing environments due to their highly

aggressive nature. Corrosion rate values were in the range of >4 mg cm^{-2} d^{-1} and ~ 4× 10^{-2} mg cm^{-2} d^{-1} in salt fog and humid atmosphere respectively.

3. After cold–pressing post–treatment of the deposited Al coatings, a significant reduction in the number of interconnected pores was observed. This resulted in more homogeneous coatings with improved bonding at the substrate/coating interface and reduced corrosion attack in saline (0.3 mg cm^{-2} d^{-1}) and high humidity (~1.3 × 10^{-2} mg cm^{-2} d^{-1}) environments. According to the gravimetric and electrochemical measurements, the corrosion behaviour of these specimens was irrespective of the composition or microstructure of the magnesium substrate and it was only associated with the corrosion of the Al coatings. A relatively thin corrosion layer consisting of β–$Al_2O_3 \cdot 3H_2O$ was observed on the outermost surface of Al–TS+CP coatings.

Acknowledgements. The authors are grateful to the MCYT (Project MAT 2006–13179–C02–02), the Community of Madrid (ESTRUMAT_CM MAT/77) for support of this work.

References

1. G. Song, A.L. Bowles, D.H. St. John, Mater. Sci. Eng. A 366, (2004): p. 74.
2. G.L. Makar, K. Kruger, J. Electrochem. Soc. 137, (1990): p. 414.
3. C.B. Baliga, P. Tsakiropoulos, Mater. Sci. Technol. 9 (1993): p. 513.
4. A. Pardo, M.C. Merino, A.E. Coy, R. Arrabal, F. Viejo, E. Matykina, Corros. Sci. 50, (2008): p. 823.
5. A. Pardo, M.C. Merino, A.E. Coy, F. Viejo, R. Arrabal, S. Feliu Jr., Electrochim. Acta 53, (2008): p. 7890.
6. G. Song, A. Atrens, Adv. Eng. Mater. 1, (1999): p. 11.
7. W.S. Loose, Corrosion and Protection of Magnesium, eds. L.M. Pidgeon, J.C. Mathes, N.E. Woldmen, (Materials Park, OH: ASM International, 1946), p. 173.
8. R. Lindström, L.-G. Johansson, J.-E. Svensson, Mater. Corros. 54, (2003): p. 587.
9. N. LeBozec, M. Jonsson, D. Thierry, Corrosion 4, (2004): p. 346.
10. N.N. Aung, W. Zhou, J. Appl. Electrochem. 32, (2002): p. 1397.
11. R. Tunold, H. Holtan, M.B. Hagg Berfe, A. Lasson, R. Steen-Hansen, Corr. Sci. 17, (1977): p. 353.
12. I.L. Rozenfeld, Atmospheric Corrosion of Metals, (Houston, NACE 1972).
13. H.P. Godard, W.B. Jepson, M.E. Bothwell, R.L. Lane, The corrosion of Light Metals, (New York, Wiley and Sons, 1967).
14. DTI Global Watch Mission Report, "MAGTECH 1: Magnesium alloys and processing technologies for lightweight transport applications-a mission to Europe 2004".
15. J.E. Gray, B. Luan, J. Alloys Compd. 336, (2002): p. 88.
16. M.A. González-Nuñez, P. Skeldon, G.E. Thompson, H. Karimzadeh, Corrosion 55, (1999): p. 1136.

17. European Union directive 2002/95/EC, Restriction of Hazardous Substances Directive.

18. C. Blawert, W. Dietzel, E. Ghali, G. Song, Adv. Eng. Mat. 8, (2006): p. 511.

19. ASM Handbook, Vol. 13: Corrosion, 9th ed. (Materials Park, OH: ASM International, 1987), p. 459.

20. J. Zhang, Y. Wang, R. Zeng, W. Huang, Mater. Sci. Forum 546-549, (2007): p. 529.

21. L.H. Chiu, C.C. Chen, C.F. Yang, Surf. Coat. Technol. 191, (2005): p. 181.

22. J. Zhang, Y. Wang, Key Eng. Mater. 373-374, (2008): p. 55.

23. W. Zhongshan, L. Liufa, D. Wenjiang, Mater. Sci. Forum 488-489, (2005): p. 685.

24. M. Shigematsu, N. Nakamura, K. Saitou, J. Mater. Sci. Letters 19, (2000): p. 473.

25. B. Wielage, T. Grund, H. Pokhmurska, C. Rupprecht, T. Lampke, Key Eng. Mater. 384, (2008): p. 99.

26. L. Chiu, H. Lin, C. Chen, C. Yang, C. Chang, J. Wu, Mater. Sci. Forum 419-422, (2003): p. 909.

27. H. Pokhmurska, B. Wielage, T. Lampke, T. Grund, M. Student, N. Chervinska, Surf. Coat. Technol. 202, (2008): p. 4515.

28. S. Feliu Jr., A. Pardo, M.C. Merino, A.E. Coy, F. Viejo, R. Arrabal, Appl. Surf. Sci. 255, (2009): p. 4102.

29. Z. Wei, L. Liu, W. Ding, Mater. Sci. Forum 488-489, (2005) p. 685.

30. L.H. Chiu, H.A. Lin, C.C. Chen, C.F. Yang, C.H. Chang, J.C. Wu, Mater. Sci. Forum 419-422, (2003): p. 909.

31. A. Pardo, M.C. Merino, R. Arrabal, F. Viejo, M. Carboneras, A.E. Coy, Corrosion 62, (2006): p. 141.

32. A. Pardo, M.C. Merino, F. Viejo, S. Feliu Jr., M. Carboneras, R. Arrabal, J. Electrochem. Soc. 152, (2005): p. B198.

33. G. Song, A. Atrens, Adv. Eng. Mater. 7, (2005): p. 563.

34. M. Jönsson, D. Persson, C. Leygraf, Corros. Sci. 50, (2008): p. 1406.

35. C.R. Southwell, A.L. Alexander, C.W. Hummer, Corrosion of metals in tropical environments – aluminium and magnesium, Materials Protection 4 (1965), p. 30.

36. M. Jönsson, D. Persson, D. Thierry, Corros. Sci. 49, (2007): p. 1540.

37. R. Lindström, L.G. Johansson, G.E. Thompson, P. Skeldon, J.E. Svensson, Corros. Sci. 46, (2004): p. 1141.

38. F. Hehmann, F. Sommer, H. Jones, R.G.J. Edyvean, J. Mater. Sci. 24 (1989): p. 2369.

39. A. Pardo, M.C. Merino, R. Arrabal, S. Merino, F. Viejo, A.E. Coy, Appl. Surf. Sci. 252, (2006): p. 2794.

40. A. Pardo, M.C. Merino, R. Arrabal, F. Viejo, M. Carboneras, J.A. Muñoz, Corros. Sci. 48, (2006): p. 3035.

41. E. Lugscheider, M. Parco, K.U. Kainer, N. Hort, Thermal Spraying of Magnesium Alloys for Corrosion and Wear Protection, Magnesium, Proceedings of the 6th International Conference Magnesium Alloys and Their Applications, K.U. Kainer ed., (Wiley-VCH Verlag GmbH & Co. 2005) p. 860.

Figure and Table Captions

Table 1. Chemical composition of investigated magnesium alloys.

Table 2. Electrochemical data of tested materials after immersion in 3.5 wt.% NaCl for 1 h.

Table 3. Differences between pitting, corrosion and repassivation potentials of the Al–TS+CP specimens after immersion in 3.5 wt.% NaCl for 1 h.

Table 4. Kinetic laws of materials exposed to salt fog environment.

Table 5. Kinetic laws of materials exposed to high humidity environment.

Figure 1. Backscattered scanning electron (BSE) micrographs of the cross–sections of: (a–c) Al–TS and (d–f) Al–TS+CP coatings (AZ31, AZ80 and AZ91D alloys).

Figure 2. Scanning electron micrographs of the surfaces and substrate/coating interfaces of (a,c) Al–TS and (b,d) Al–TS+CP specimens.

Figure 3. Polarization curves of tested materials after immersion in 3.5 wt.% NaCl for 1 h at room temperature.

Figure 4. Mass gain vs. immersion time for the materials exposed to salt fog environment.

Figure 5. Mass gain vs. immersion time for the materials exposed to high humidity (98% RH at 50 ^{o}C) environment.

Figure 6. SEM micrographs of the plan views of the AZ31 and AZ80 alloys after 21 days of exposure to salt fog atmosphere. (a,b) Untreated; (c,d) Al–TS and (e,f) Al–TS+CP specimens.

Figure 7. BSE micrograph of the cross–section of the AZ80 alloy after exposure to salt fog for 21 days.

Figure 8. BSE micrograph and X-ray elemental maps of Mg, Al and O of the AZ91 alloy with the Al–TS coating after exposure to salt fog for 21 days.

Figure 9. BSE micrograph and EDX profile of the cross-section of the AZ91D alloy with the Al–TS+CP coating after exposure to salt fog for 21 days.

Figure 10. Low angle XRD (incident angle 1°) study of tested materials exposed to salt fog environment for 21 days (a) Untreated; (b) Al–TS and (c) Al–TS+CP specimens.

Figure 11. SEM micrographs of the plan views of the AZ31 and AZ80 alloys after 28 days of exposure to high humidity environment. (a,b) Untreated; (c,d) Al–TS and (e,f) Al–TS+CP specimens.

Figure 12. Low angle XRD (incident angle 1°) study of tested materials exposed to high humidity environment for 28 days (a) Untreated; (b) Al–TS and (c) Al–TS+CP specimens.

Figure 13. pH values of the 3.5 wt.% solution after immersion of the investigated specimens for 1h.

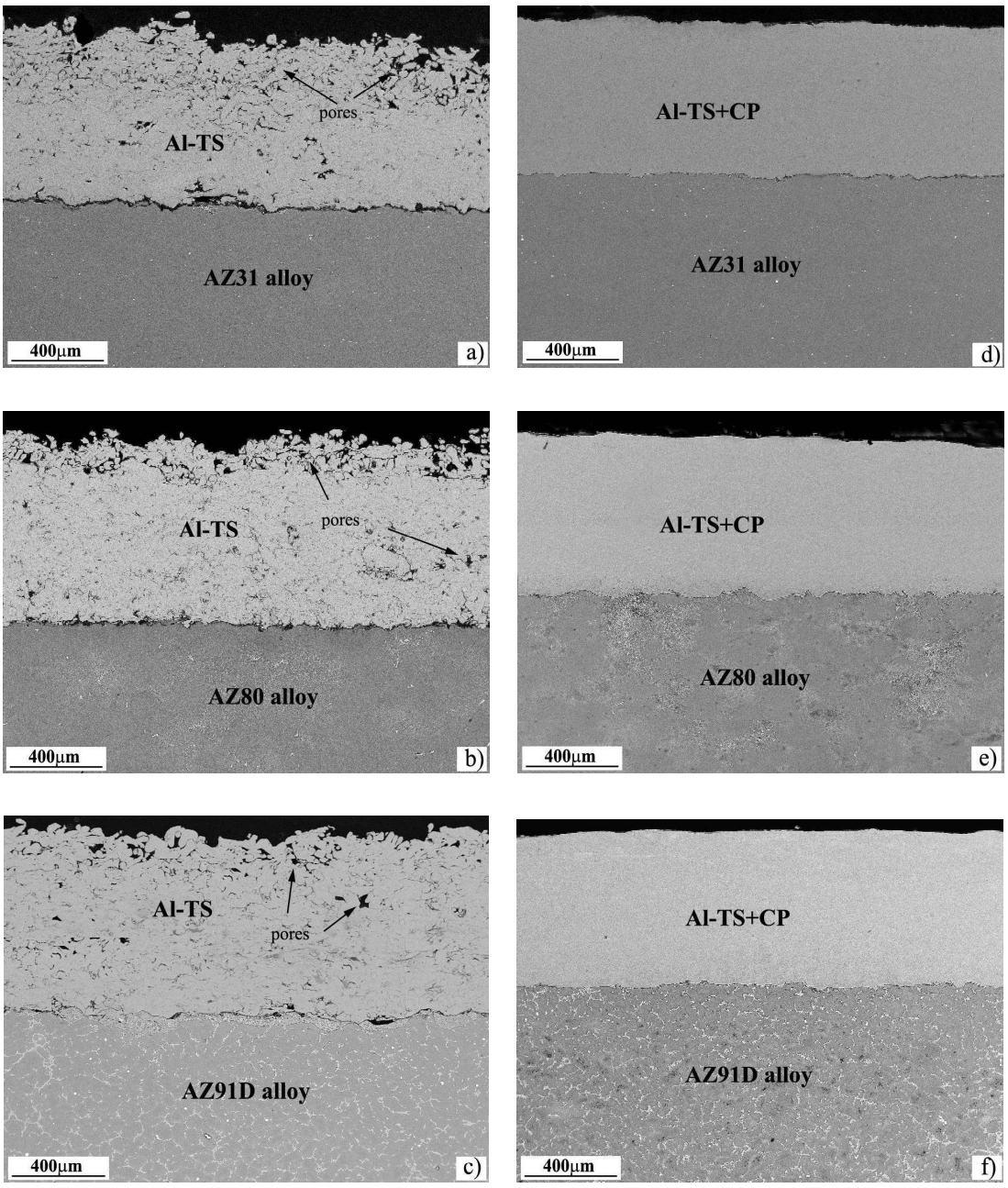
Al-TS
pores
AZ31 alloy
400μm
a)
Al-TS+CP
AZ31 alloy
400μm
d)
Al-TS
pores
AZ80 alloy
400μm
b)
Al-TS+CP
AZ80 alloy
400μm
e)
Al-TS
pores
AZ91D alloy
400μm
c)
Al-TS+CP
AZ91D alloy
400μm
f)

Figure 1

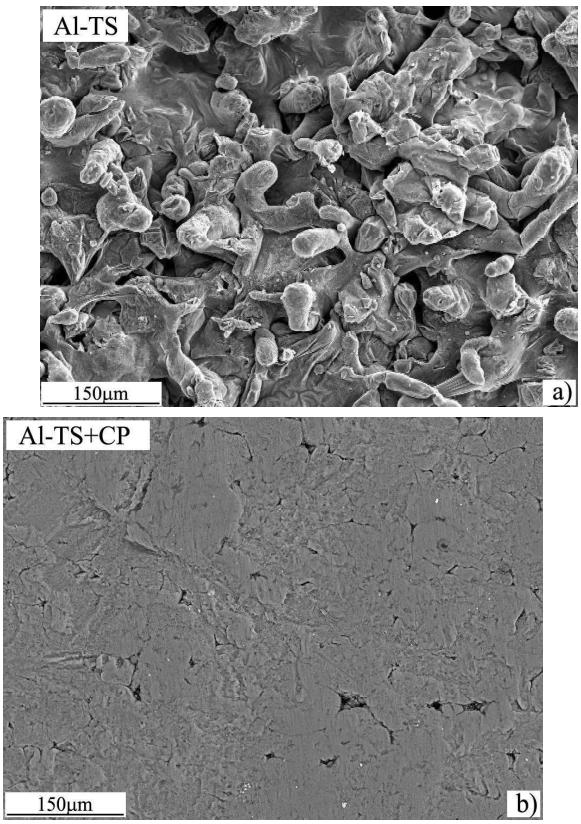
Al-TS
150μm
a)
Al-TS+CP
150μm
b)
Al-TS
AZ31 alloy
Al-Mn
40μm
c)
Al-TS+CP
AZ31 alloy
Al-Mn
40μm
d)

Figure 2

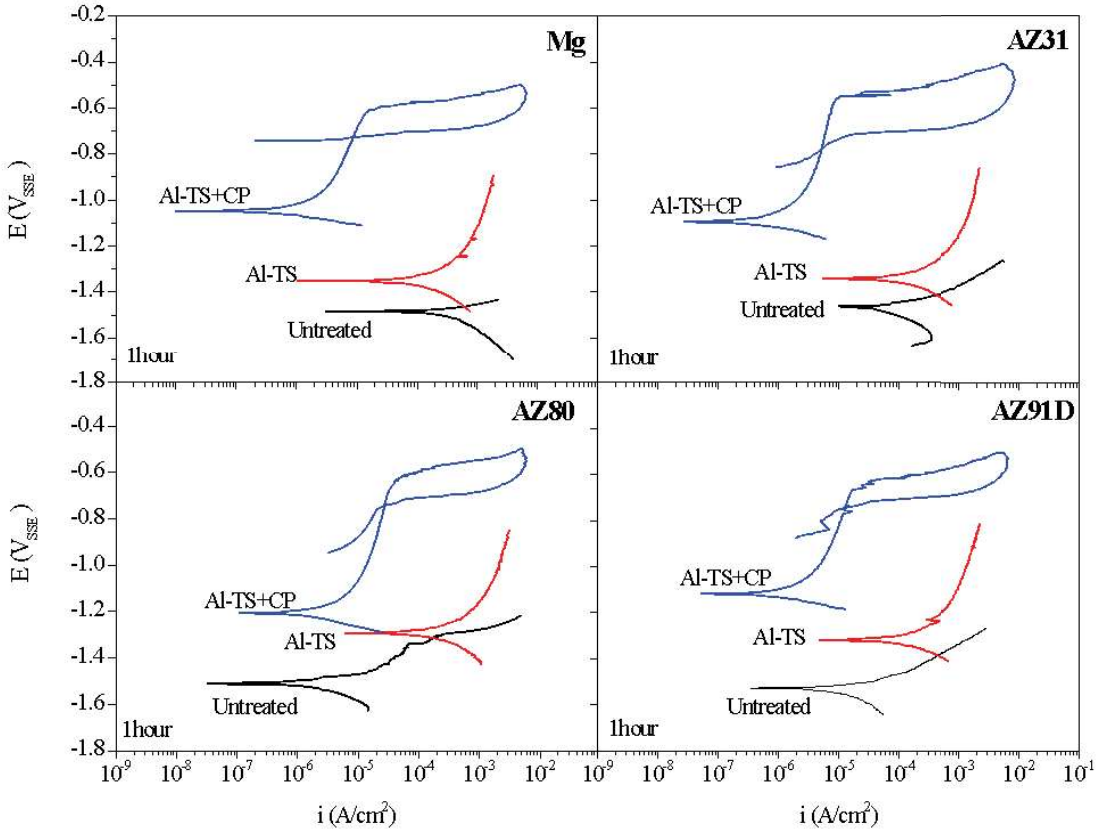

Figure 3

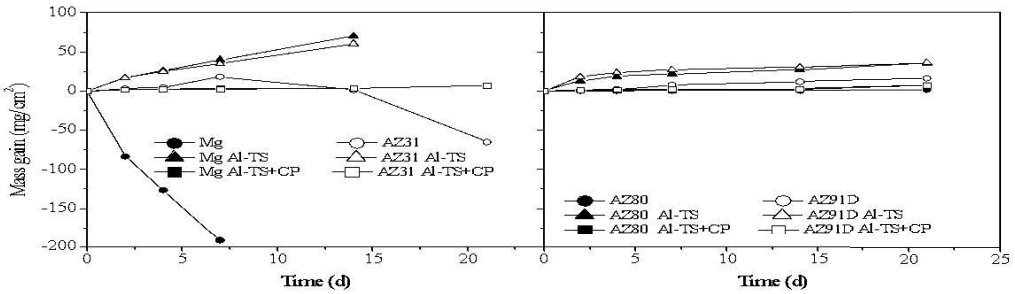

Figure 4

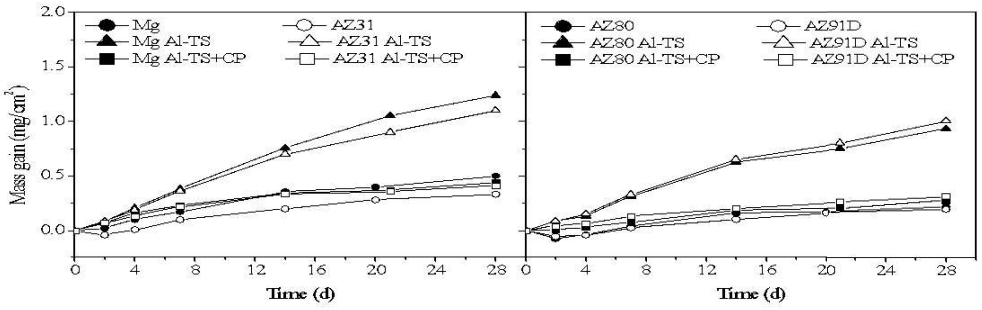

Figure 5

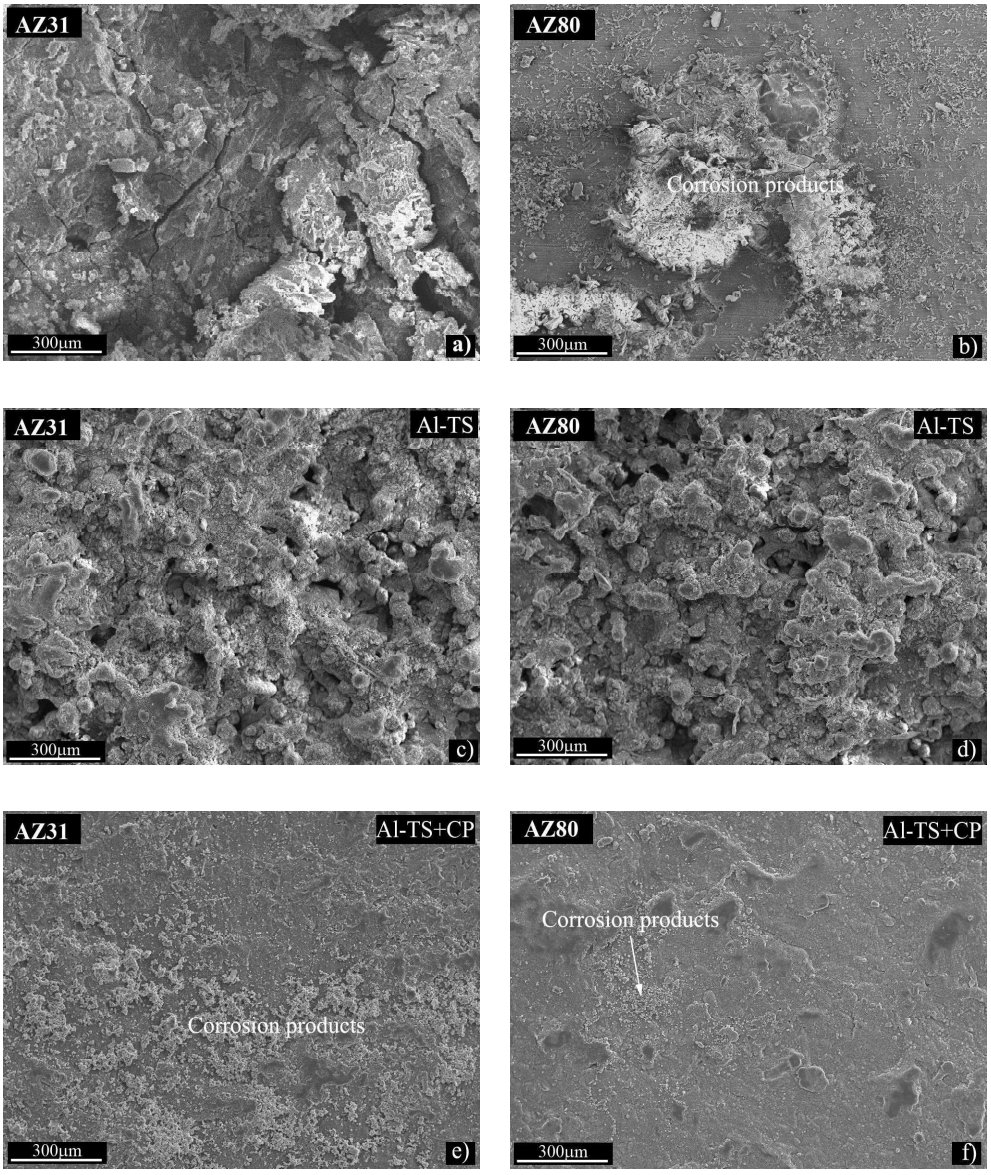
AZ31
300μm
a)
AZ80
Corrosion products
300μm
b)
AZ31
Al-TS
300μm
c)
AZ80
Al-TS
300μm
d)
AZ31
Al-TS+CP
Corrosion products
300μm
e)
AZ80
Al-TS+CP
Corrosion products
300μm
f)

Figure 6

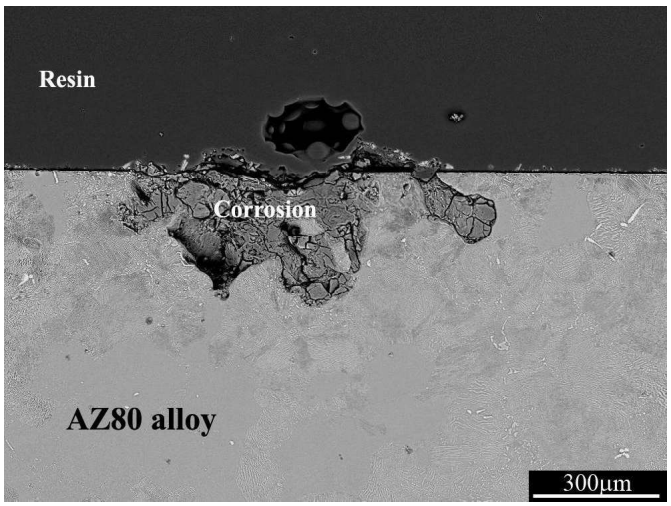

Figure 7

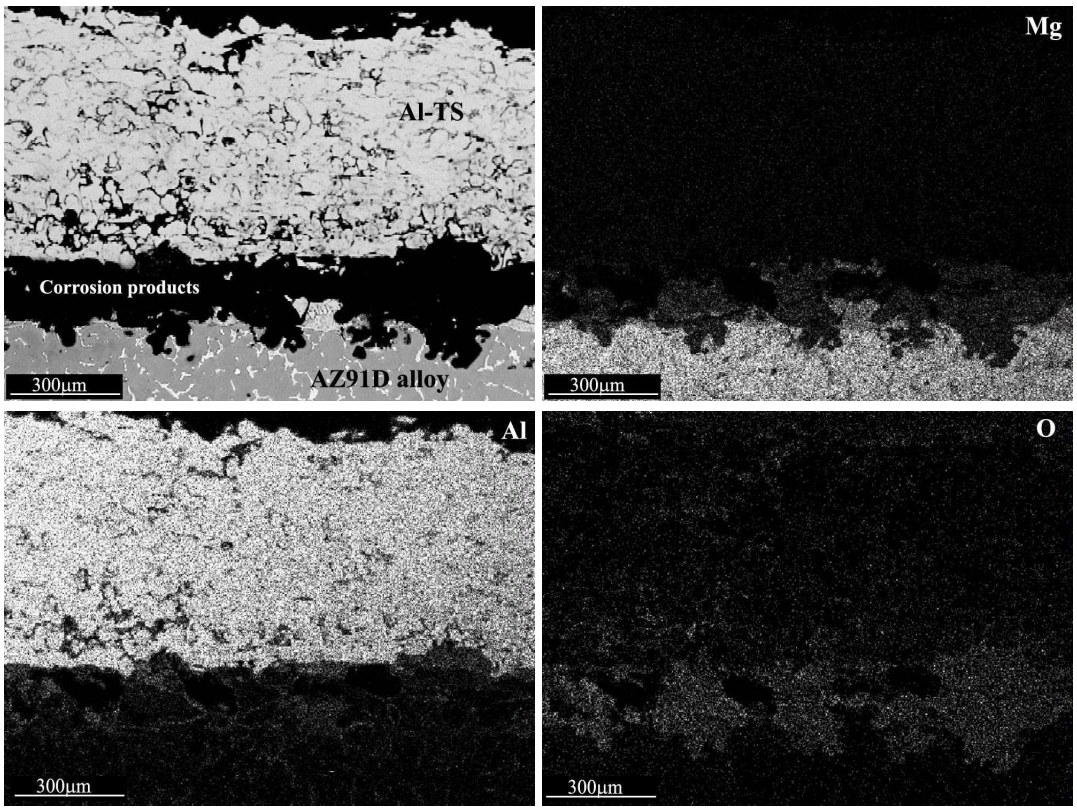

Figure 8

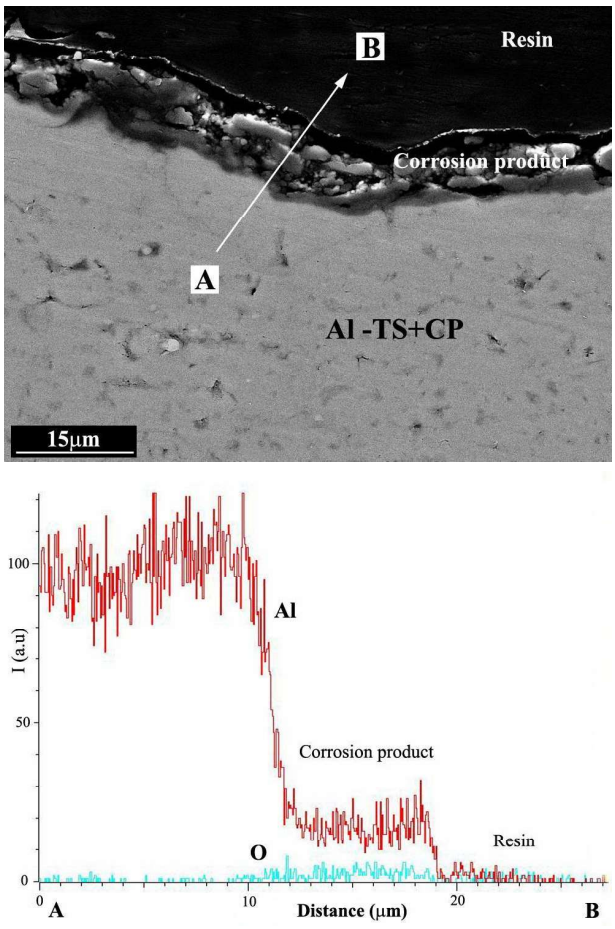
B
Resin
Corrosion product
A
Al -TS+CP
15μm
100
50
0
I (a.u)
Al
Corrosion product
O
Resin
0
10
20
A
Distance (μm)
B

Figure 9

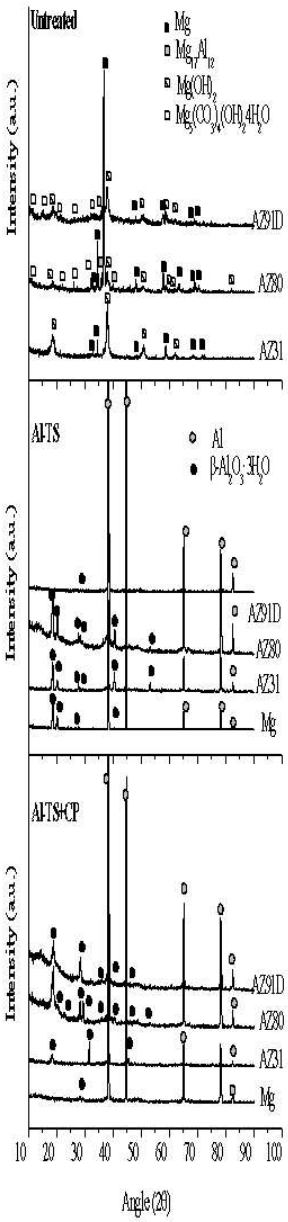
Untreated
Mg
Mg17Al12
Mg(OH)2
Mg5(CO3)4(OH)2·4H2O
AZ91D
AZ80
AZ31
Intensity (a.u.)
Al-TS
Al
β-Al2O3·3H2O
AZ91D
AZ80
AZ31
Mg
Intensity (a.u.)
Al-TS+CP
AZ91D
AZ80
AZ31
Mg
Intensity (a.u.)
10 20 30 40 50 60 70 80 90 100
Angle (2θ)

Figure 10

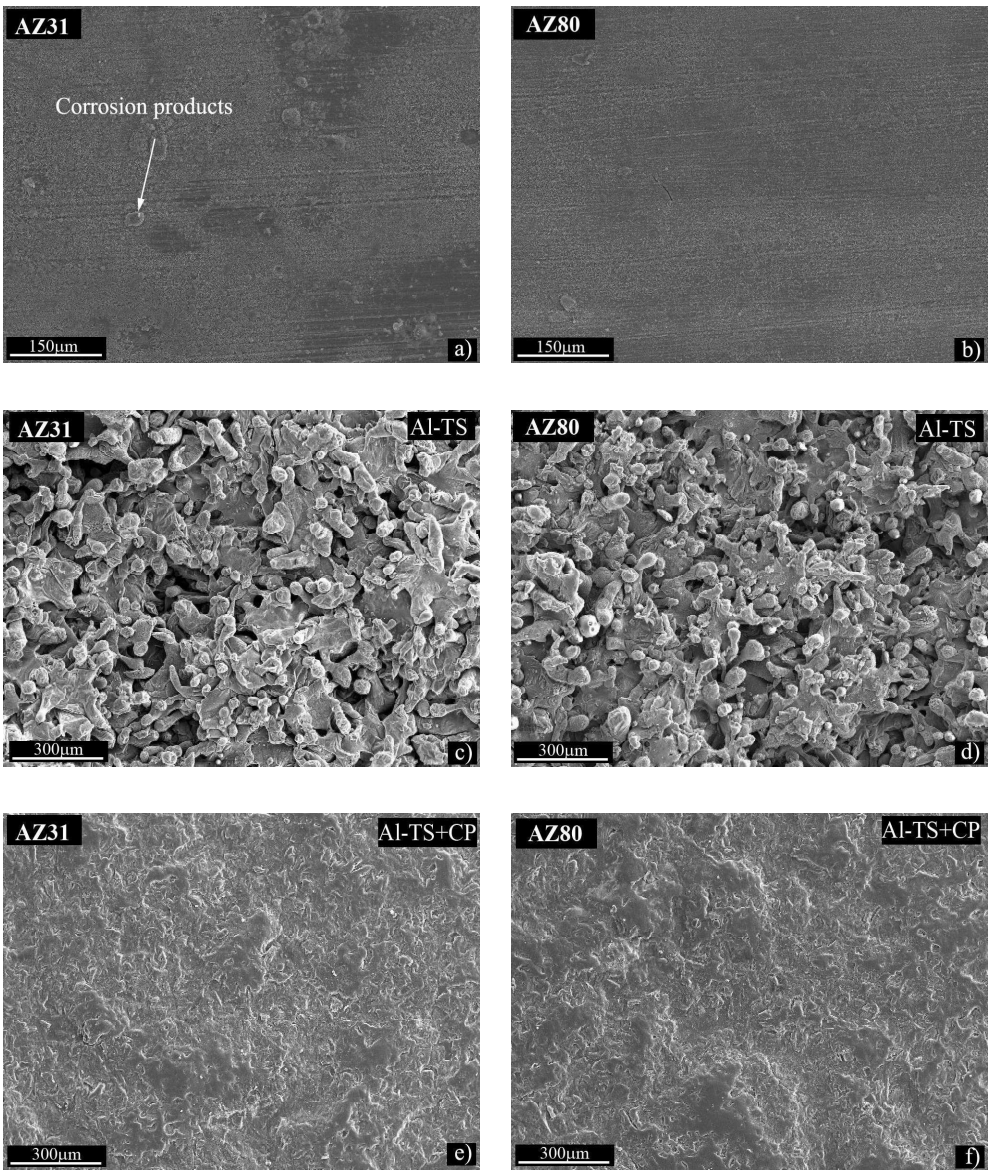
AZ31
Corrosion products
150μm
a)
AZ80
150μm
b)
AZ31
Al-TS
300μm
c)
AZ80
Al-TS
300μm
d)
AZ31
Al-TS+CP
300μm
e)
AZ80
Al-TS+CP
300μm
f)

Figure 11

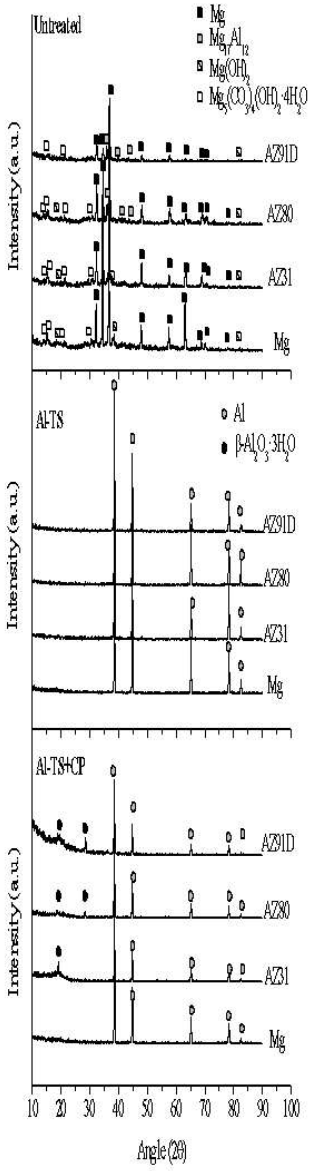
Untreated
Mg
Mg17Al12
Mg(OH)2
Mg5(CO3)4(OH)2·4H2O
AZ91D
AZ80
AZ31
Mg
Intensity (a.u.)
Al-TS
Al
β-Al2O3·3H2O
AZ91D
AZ80
AZ31
Mg
Intensity (a.u.)
Al-TS+CP
AZ91D
AZ80
AZ31
Mg
Intensity (a.u.)
10 20 30 40 50 60 70 80 90 100
Angle (2θ)

Figure 12

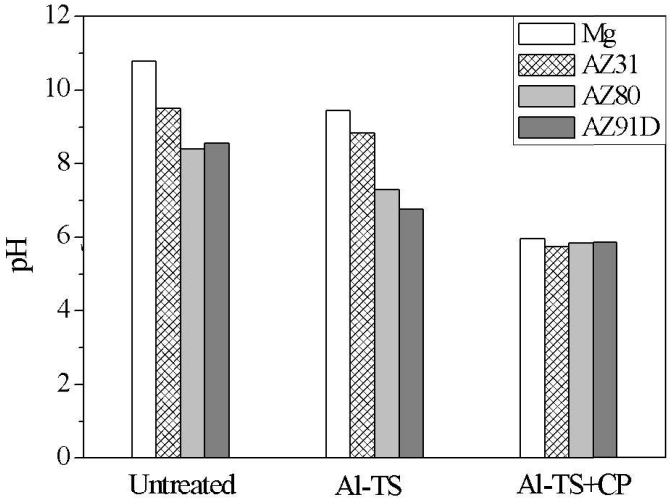

Figure 13

Material	Chemical composition (wt.%)									
	Al	**Zn**	**Mn**	**Si**	**Cu**	**Fe**	**Ni**	**Ca**	**Zr**	**Others**
Mg (99%)	0.006	0.014	0.03	0.019	0.001	0.004	<0.001			
AZ31	3.1	0.73	0.25	0.02	<0.001	0.005	<0.001	<0.01	<0.001	<0.30
AZ80	8.2	0.46	0.13	0.01	<0.001	0.004				<0.30
AZ91D	8.8	0.68	0.30	0.01	<0.001	0.004	<0.008			<0.30

Table 1

Material	E_{corr} (V_{SSE})	E_{pit} (V_{SSE})	E_{rep} (V_{SSE})	R_p(Ω cm^2)	i_{corr}(A cm^{-2})
Mg	-1.549	-	-	23	4.30×10^{-3}
Mg TS	-1.353	-	-	116	1.07×10^{-4}
Mg TS+CP	-1.098	-0.61	-0.74	16300	6.43×10^{-6}
AZ31	-1.465	-	-	349	1.38×10^{-4}
AZ31 TS	-1.343	-	-	174	1.67×10^{-4}
AZ31 TS+CP	-1.096	-0.58	-0.77	17400	6.17×10^{-6}
AZ80	-1.511	-	-	5293	1.53×10^{-5}
AZ80 TS	-1.294	-	-	184	1.06×10^{-4}
AZ80 TS+CP	-1.112	-0.61	-0.75	14000	6.02×10^{-6}
AZ91D	-1.529	-	-	1305	2.54×10^{-5}
AZ91D TS	-1.321	-	-	180	1.23×10^{-4}
AZ91D TS+CP	-1.122	-0.62	-0.75	15000	6.56×10^{-6}

Table 2

Material	E_{pit}-E_{corr} (V_{SSE})	E_{pit}-E_{rep} (V_{SSE})	E_{rep}-E_{corr} (V_{SSE})
Mg TS+CP	0.49	0.13	0.36
AZ31 TS+CP	0.51	0.19	0.33
AZ80 TS+CP	0.51	0.14	0.37
AZ91D TS+CP	0.50	0.13	0.37

Table 3

Material	Kinetic law: $y = b \cdot t / y^2 = b \cdot t$; [y (mg/cm^2), t (d)]		r^2
Mg (99%)	$y = -55t$	$0 \leq t \leq 2$	1
Mg TS	$y = 4.8t$	$0 \leq t \leq 14$	0.99
Mg TS+CP	$y = 0.3t$	$0 \leq t \leq 21$	0.96
AZ31	$y = 2.8t$	$0 \leq t \leq 7$	0.95
	$y = -8.7t$	$7 \leq t \leq 21$	0.99
AZ31 TS	$y = 4.0t$	$0 \leq t \leq 14$	0.99
AZ31 TS+CP	$y = 0.3t$	$0 \leq t \leq 21$	0.97
AZ80	$y = 0.2t$	$0 \leq t \leq 21$	0.98
AZ80 TS	$y^2 = 41.8t$	$0 \leq t \leq 21$	0.98
AZ80 TS+CP	$y = 0.3t$	$0 \leq t \leq 21$	0.93
AZ91D	$y = 1.55t$	$0 \leq t \leq 21$	0.99
AZ91D TS	$y^2 = 28.3t$	$0 \leq t \leq 21$	0.98
AZ91D TS+CP	$y = 0.3t$	$0 \leq t \leq 21$	0.97

Table 4

Material	Kinetic law : $y = b \cdot t$; [y (mg/cm^2), t (d)]		r^2
Mg (99%)	$y = 1.9 \times 10^{-2} t$	$0 \leq t \leq 28$	0.95
Mg TS	$y = 4.6 \times 10^{-2} t$	$0 \leq t \leq 28$	0.98
Mg TS+CP	$y = 1.6 \times 10^{-2} t$	$0 \leq t \leq 28$	0.96
AZ31	$y = 1.7 \times 10^{-2} t$	$0 \leq t \leq 28$	0.94
AZ31 TS	$y = 4.0 \times 10^{-2} t$	$0 \leq t \leq 28$	0.98
AZ31 TS+CP	$y = 1.4 \times 10^{-2} t$	$0 \leq t \leq 28$	0.94
AZ80	$y = 1.2 \times 10^{-2} t$	$0 \leq t \leq 28$	0.95
AZ80 TS	$y = 3.4 \times 10^{-2} t$	$0 \leq t \leq 28$	0.97
AZ80 TS+CP	$y = 1.0 \times 10^{-2} t$	$0 \leq t \leq 28$	0.96
AZ91D	$y = 1.3 \times 10^{-2} t$	$0 \leq t \leq 28$	0.98
AZ91D TS	$y = 3.5 \times 10^{-2} t$	$0 \leq t \leq 28$	0.97
AZ91D TS+CP	$y = 1.0 \times 10^{-2} t$	$0 \leq t \leq 14$	0.96

Table 5